PNAS RESEARCH ARTICLE | NEUROSCIENCE

A small molecule M1 promotes optic nerve regeneration to restore target-specific neural activity and visual function

Ngan Pan Bennett Au[a], Raza Chand[a], Gajendra Kumar[a], Pallavi Asthana[a], Wing Yip Tam[a], Kin Man Tang[b], Chi-Chiu Ko[b], and Chi Him Eddie Ma[a,1]

Edited by Thomas Schwarz, Harvard Medical School, Boston, MA; received December 1, 2021; accepted August 31, 2022 by Editorial Board Member Jeremy Nathans

Axon regeneration is an energy-demanding process that requires active mitochondrial transport. In contrast to the central nervous system (CNS), axonal mitochondrial transport in regenerating axons of the peripheral nervous system (PNS) increases within hours and sustains for weeks after injury. Yet, little is known about targeting mitochondria in nervous system repair. Here, we report the induction of sustained axon regeneration, neural activities in the superior colliculus (SC), and visual function recovery after optic nerve crush (ONC) by M1, a small molecule that promotes mitochondrial fusion and transport. We demonstrated that M1 enhanced mitochondrial dynamics in cultured neurons and accelerated in vivo axon regeneration in the PNS. Ex vivo time-lapse imaging and kymograph analysis showed that M1 greatly increased mitochondrial length, axonal mitochondrial motility, and transport velocity in peripheral axons of the sciatic nerves. Following ONC, M1 increased the number of axons regenerating through the optic chiasm into multiple subcortical areas and promoted the recovery of local field potentials in the SC after optogenetic stimulation of retinal ganglion cells, resulting in complete recovery of the pupillary light reflex, and restoration of the response to looming visual stimuli was detected. M1 increased the gene expression of mitochondrial fusion proteins and major axonal transport machinery in both the PNS and CNS neurons without inducing inflammatory responses. The knockdown of two key mitochondrial genes, *Opa1* or *Mfn2*, abolished the growth-promoting effects of M1 after ONC, suggesting that maintaining a highly dynamic mitochondrial population in axons is required for successful CNS axon regeneration.

axon regeneration | mitochondrial dynamics | peripheral nerve injury | optic nerve crush | visual function recovery

Significance

Retinal ganglion cells typically fail to regenerate injured axons after injury, leading to permanent visual loss after optic nerve damage. Activation of intrinsic growth capacity, an energy-demanding process, facilitates axonal regrowth from injured neurons. Here, we demonstrate that M1, a small molecule that promotes mitochondrial fusion and motility, enhances intrinsic growth capacity of injured neurons and accelerates in vivo axon regeneration of injured neurons. More strikingly, M1 treatment sustains long-distance axon regeneration from optic chiasm to multiple subcortical visual targets in the brain. Regenerated axons elicit neural activities in target brain regions and restore pupillary light reflex and responses to looming visual stimuli. Our study highlights the potential of nonviral, mitochondria-based therapy for nervous system repair.

Despite substantial efforts to improve clinical outcomes over the past two decades, nervous system injuries remain the leading cause of disability worldwide. In the adult mammalian central nervous system (CNS), neurons fail to regenerate their axons after injury largely because of the hostile microenvironment and the lack of intrinsic growth capacity. Progress has been made in facilitating axon regeneration by modifying the microenvironment surrounding the CNS either through neutralizing inhibitory molecules (1), an approach that remains largely elusive (2, 3), or by the genetic modification of neurons (4–7), namely the overexpression or deletion of regeneration-associated genes (RAGs) (4–7), which tends to promote considerable axon regeneration. Although the concept of gene therapy seems to be straightforward, its routine clinical implementation requires the development of more efficient methods to deliver transgenes specifically to target tissues with high transduction efficiency (8). Genetic modification may lead to adverse effects, such as uncontrolled cell proliferation with malignant potential (9). Consequently, there is an urgent need to identify factors, such as small molecules that can serve as a ready-to-use therapy, that can activate the intrinsic growth capacity of injured neurons. Additionally, understanding the processes and mechanisms that underlie axon regeneration in the peripheral nervous system (PNS) may contribute to facilitating regeneration in the CNS.

Axon regeneration is an energy-demanding process that requires active mitochondrial transport and movement (6, 10). In contrast to the CNS, axonal mitochondrial transport in regenerating PNS axons increases within hours of injury and can be sustained for weeks (11). Mitochondria undergo frequent fusion, fission, and bidirectional axonal transport for the exchange of mitochondrial DNA, proteins, and metabolites. A balance between fusion and fission determines the size and length of mitochondria (12). Substantial efforts have been devoted to understanding mitochondrial dynamics in the CNS and PNS over recent years. In vivo imaging has demonstrated that mitochondria are mostly stationary in uninjured peripheral axons. The transection of peripheral axons

Author contributions: N.P.B.A. and C.H.E.M. designed research; N.P.B.A., R.C., G.K., P.A., W.Y.T., and K.M.T. performed research; N.P.B.A., R.C., G.K., P.A., W.Y.T., C.-C.K., and C.H.E.M. analyzed data; and N.P.B.A. and C.H.E.M. wrote the paper.

The authors declare no competing interest.

This article is a PNAS Direct Submission. T.S. is a guest editor invited by the Editorial Board.

[1]To whom correspondence may be addressed. Email: eddiema@cityu.edu.hk.

This article contains supporting information online at http://www.pnas.org/lookup/suppl/doi:10.1073/pnas.2121273119/-/DCSupplemental.

Published October 28, 2022.

of dorsal root ganglion (DRG) neurons in the PNS followed by a second lesion to the central axons of these neurons in the spinal cord 1 wk later was shown to promote the regrowth of the transected central axons into and beyond the lesion site, which is known as the "conditioning effect" (13, 14). Indeed, preconditioned neurons exhibited faster axonal mitochondrial transport in both central and peripheral regenerating branches, whereas axonal mitochondrial transport was markedly reduced in DRG neurons after spinal cord injury alone (15). Ablation of the genes encoding the mitochondrial transport proteins Miro or DLK-1 reduced both mitochondrial density and transport in regenerating axons, leading to poor axon regeneration (10). In mice, knocking out syntaphilin (*snph*), which encodes an anchoring protein that immobilizes neuronal mitochondria, led to a substantial increase in the percentage of motile axonal mitochondria (~70%), which resulted in enhanced regenerative capacity (16). Interestingly, *snph* expression was found to be tightly regulated in the CNS in a development-dependent manner, with a peak of expression in adults and hardly detectable expression levels in the embryonic stages (17). These observations are consistent with the long-held dogma that axonal growth capacity is substantially diminished as neurons mature (14, 18) and further suggest that decline in mitochondrial dynamics contributes to the lack of neuronal regenerative capacity in the CNS. Yet, little is known about targeting mitochondria in nervous system repair.

Here, we first demonstrate that M1, a small molecule that modulates axonal mitochondrial dynamics (19), accelerates axonal mitochondrial transport and enhances in vivo axon regeneration in injured peripheral neurons. Remarkably, M1 treatment induced substantial local field potentials (LFPs) in the superior colliculus (SC) following optogenetic stimulation of retinal ganglion cells (RGCs) by increasing the number of axons regenerating through the optic chiasm into the multiple subcortical visual targets 6 wk after optic nerve crush (ONC). This resulted in the complete recovery of the pupillary light reflex (PLR) and the complete restoration of the response to looming visual stimuli in nearly half of the mice. We further confirmed the robust M1-induced regenerative capacity of injured RGCs by tracing axonal sprouting along the optic tract using an anterograde tracer cholera toxin subunit B (CTB). Finally, we found that M1 increased the gene expression of mitochondrial fusion proteins and major axonal transport machinery in both the PNS and CNS neurons without inducing inflammatory responses. In vivo adeno-associated virus 2 (AAV2)–mediated silencing of two key mitochondrial genes, *Opa1* or *Mfn2*, in the retina completely abolished the regeneration-promoting effect of M1. These findings emphasize the potential of modulating mitochondrial dynamics to promote axon regeneration and identify M1, a readily available small molecule, as a putative therapeutic drug for the treatment of nerve injury.

Results

M1 Modulates Mitochondria Dynamics and Accelerates Peripheral Axon Regeneration. Accumulating evidence suggests that axonal mitochondrial dynamics plays a key role in axon regeneration (6, 10, 11, 15). We, therefore, performed a series of proof-of-concept experiments to test the therapeutic potential of a mitochondrial fusion promoter small molecule M1 (19) in promoting axon regeneration. We first examined whether M1 could induce mitochondrial fusion, accelerate axonal mitochondrial motility and transport velocity, and thereby, enhance axon regeneration. We found that M1 induced a 25% increase in mitochondrial size in the distalmost portions of axons of adult DRG neurons relative to that in vehicle-treated controls (Fig. 1*A*), as evidenced by the significant increase in the cumulative frequency of larger mitochondria in M1-treated DRG neurons ($d = 0.187$, $P < 0.001$) (Fig. 1*B*). In vehicle-treated DRG neurons, mitochondrial fusion proteins, such as OPA1 (Fig. 1*C* and *SI Appendix*, Fig. S1*A*) and MFN2 (Fig. 1*D* and *SI Appendix*, Fig. S1*B*), were evenly distributed along the axon shafts and growth cones. In contrast, in M1-treated DRG neurons, OPA1 and MFN2 immunoreactivity was strongest in the filopodial protrusions (growth cones) and colocalized with actin at the filopodia, where active actin polymerization occurs during neurite extension (14) (Fig. 1*E*). M1 treatment increased the expression of OPA1 and MFN2 at both the messenger ribonucleic acid (mRNA) (6.5- and 15-fold, respectively) (Fig. 1*F*) and protein (2- and 1.4-fold, respectively) levels in the mitochondrial fractions of DRG neurons (Fig. 1*G*).

To investigate the effect of M1 on axonal mitochondrial transport motility and velocity, we performed live-cell imaging on MitoTracker Red–stained mouse DRG neurons. A series of time-lapse images was collected between 6.5 and 9 h after cell plating, a time point where active neurite extension occurs in cultured DRG neurons (20–23). Kymograph analysis of mitochondrial movements revealed that M1 treatment increased the motile pool of mitochondria significantly when compared with vehicle control (Fig. 2 *A* and *B*), although the mitochondrial density in the distalmost axonal segments remained unchanged (Fig. 2*C*). Furthermore, M1 increased the fraction of time that mitochondria spent in motion rather than remaining stationary (Fig. 2*D*). The average axonal mitochondrial transport velocity was increased by 62.5% in M1-treated neurons (0.47 ± 0.02 μm/s) when compared with vehicle control (0.29 ± 0.01 μm/s) (Fig. 2*E*). M1 administration also led to an increase in the mRNA expression levels of key genes involved in anterograde and retrograde axonal transport, such as *Kif5a*, *Miro1*, *Milton*, *Dync1h1*, and *Dctn1* (Fig. 2*F*).

Accordingly, we asked whether M1-induced mitochondrial dynamics could promote axon regeneration in the PNS. Strikingly, M1 promoted a marked increase in neurite outgrowth at relatively low doses (0.5 to 2.5 μM); however, no further neurite outgrowth was observed at higher doses (5 to 10 μM) (Fig. 2*G*). Cell survival was not affected during culture at the various concentrations used (*SI Appendix*, Fig. S2). Compared with vehicle-treated controls, the administration of M1 at the 2.5 μM concentration increased maximal neurite outgrowth from DRG neurons by 44.2% (Fig. 2 *H* and *I*). These results indicated that there is a clear link between mitochondrial dynamics and axonal regrowth.

The main limitation on PNS axon regeneration is the slow rate of regrowth, typically limited to around 1 mm/d in humans and rodent (14, 24). We, therefore, extended these findings to in vivo studies of axon regeneration after sciatic nerve crush (SNC) with the nerve pinch test in mice (Fig. 3*A*). Under light anesthesia, a series of pinches was applied directly to the injured nerves from the most distal part (trifurcation) moving proximally toward the crush site using a smooth forceps. The regeneration distance was measured from the crush site to the most distal point of the nerve that produced a reflex withdrawal when pinched (14, 18). Consistently, axon growth of vehicle-treated mice extended as far as 3.08 ± 0.10 mm at day 3 post-SNC, indicating limited axonal regrowth. Notably, lengthy axon regeneration (5.12 ± 0.05 mm) was observed with the administration of M1, which increased the most distal axon regrowth by 65.8% (Fig. 3*B*). The in vivo growth-promoting effects of M1 were

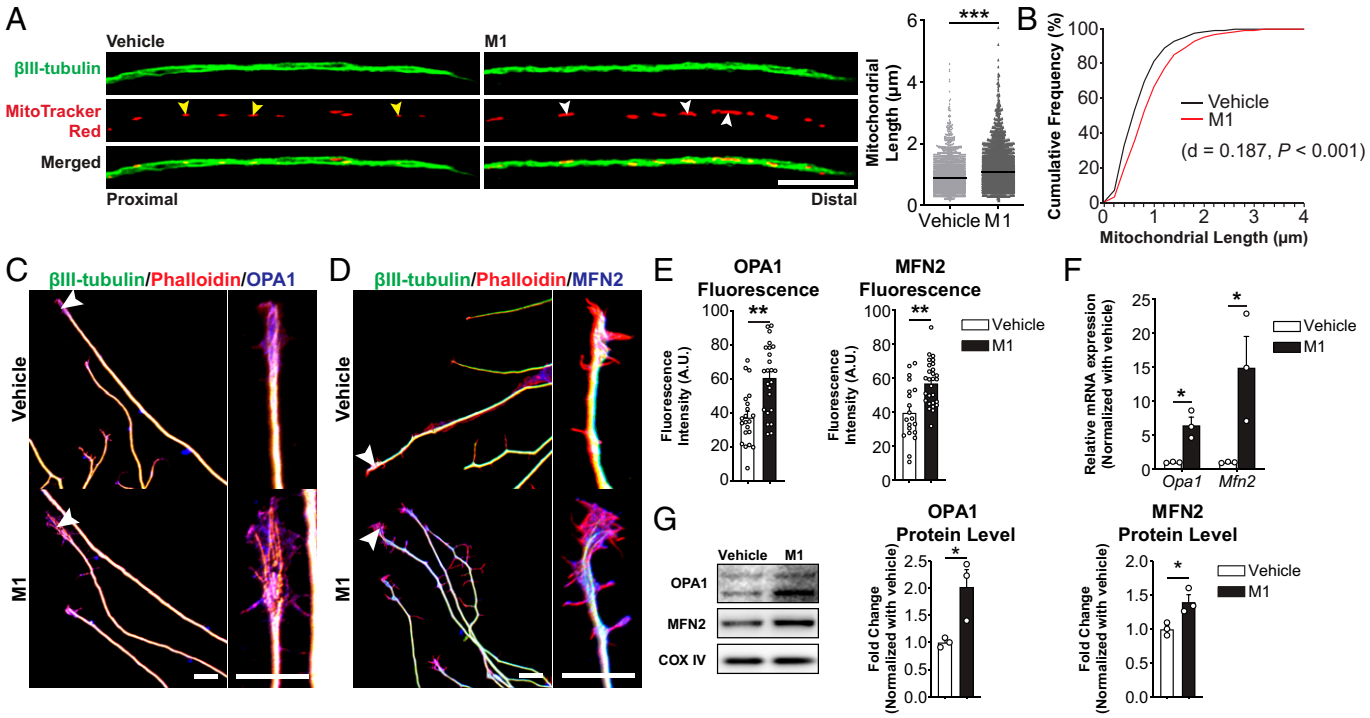

Fig. 1. M1 increases axonal mitochondrial length and expression of key mitochondrial fusion proteins in cultured adult DRG neurons. (*A*) Representative fluorescence micrographs of distal axonal segments of DRG neurons showing that there was a marked increase in mitochondrial clustering and size after M1 treatment. Yellow arrowheads indicate individual mitochondria; white arrowheads indicate clustered mitochondria. The graph depicts mitochondrial length; there was a significant increase in mitochondrial size in M1-treated (2.5 μM) neurons compared with vehicle-treated controls (0.1% dimethyl sulphoxide; DMSO). A total of 3,291 (vehicle treatment) and 2,988 (M1 treatment) mitochondria from three independent cell cultures were evaluated. Each dot represents one mitochondrion. Data points are shown in gray; the median is indicated as a black line. (*B*) M1 (2.5 μM) induced a significant increase in the cumulative frequency of larger mitochondria in DRG neurons. (*C* and *D*) DRG neurons were costained with phalloidin to detect filopodia (red) and with βIII-tubulin (green) to identify axons. In vehicle-treated DRG neurons, OPA1 (blue; *C*) or MFN2 (blue; *D*) was evenly distributed along the axons; however, both proteins were heavily localized to the growth cones (filopodia) of regenerating axons in neurons treated with M1 (2.5 μM). White arrowheads indicate OPA1 or MFN2 localization in filopodia. Photomicrographs of individual fluorescence filters are shown in *SI Appendix*, Fig. S1. (Scale bars: 10 μm in *A*, *C*, and *D*.) (*E*) The growth cone area was outlined and defined as a region of interest (ROI). OPA1 and MFN2 fluorescence intensity (arbitrary units; A.U.) was measured within the ROI using ImageJ software. OPA1 and MFN2 immunoreactivity was markedly increased in the growth cones of M1-treated (2.5 μM) DRG neurons. Each dot represents one growth cone. (*F*) The mRNA expression levels of both *Opa1* and *Mfn2* were markedly increased compared with vehicle-treated controls (0.1% DMSO). Each dot represents the mRNA expression from one independent cell culture experiment. (*G*) M1 treatment up-regulated OPA1 and MFN2 protein expression in the mitochondrial fraction of DRG neurons. OPA1 and MFN2 expression in mitochondria was normalized to that of cytochrome c oxidase subunit IV (COX IV). Each dot represents the protein expression from one independent cell culture experiment. Adult DRG neurons were prepared from C57BL/6 mice (8 to 12 wk). Data are presented as means ± SEM from six to eight independent experiments in *A* and *B* and as means ± SEM of triplicates in *E*–*G*. The Mann–Whitney *U* test (*A*), the two-sample Kolmogorov–Smirnov test (*B*), and the Student's *t* test (*E*–*G*) were used. **P* < 0.05; ***P* < 0.01; ****P* < 0.001.

further validated by immunostaining for superior cervical ganglion 10 (SCG10), a marker for regenerating sensory axons (25, 26), which showed accelerated axon regeneration in the M1-treated mice. SCG10 immunoreactivity was prominent even in the far-distal region of the crushed nerve in the M1-treated mice (Fig. 3*C*). SCG10 immunoreactivity in the longitudinal section of the sciatic nerve was measured and normalized to the crush site referred to as the regeneration index (Fig. 3*D*) (25, 26).

To exclude inflammation as a potential contributing mechanism to the M1-promoting effect on axon regeneration, we systemically evaluated inflammatory responses by immunohistochemistry, gene expression study, and mouse cytokine array analysis. We first immunostained lumbar 4/5 (L4/5) DRGs (directly supply the sciatic nerve) and sciatic nerves (near to the crush site) cryosections with anti-F4/80 (macrophages/microglia marker) and anti–Gr-1 (neutrophils marker) antibodies harvested on early time points (days 1 and 3) after SNC and in vivo administration of M1. SNC injury induced a dramatic increase in F4/80-positive macrophages/microglia in the DRGs and sciatic nerves at days 1 and 3 postinjury (27), while the administration of vehicle or M1 did not induce any infiltration of F4/80-positive cells (macrophages/microglia) into the uninjured DRGs/sciatic nerves. More importantly, M1 administration did not augment the inflammatory response by increasing the number of infiltrating F4/80-positive cells in the DRGs and sciatic nerves at days 1 and 3 post-SNC, respectively (*SI Appendix*, Fig. S3 *A* and *B*). Similarly, we observed a very low number of Gr-1–positive neutrophils in the uninjured/injured L4/5 DRGs after M1 or vehicle treatment (*SI Appendix*, Fig. S3*C*). On day 1 after SNC, there was a surge in neutrophil infiltration into the site of injury of sciatic nerves (27). M1 administration did not increase the numbers of infiltrating neutrophils further at days 1 and 3 post-SNC (*SI Appendix*, Fig. S3*D*). We then examined the gene expression of key inflammatory mediators, such as proinflammatory cytokines (*Tnf-α*, *Il-1β*, *Il-6*, *Cd86*, and *Nos2*), antiinflammatory cytokines (*Il-4*, *Il-10*, *Cd206*, *Tgf-β*, and *Igf-1*), and chemokines (*Ccl2*, *Ccl3*, *Ccl4*, and *Ccl5*), in DRGs (*SI Appendix*, Fig. S4*A*). None of these genes were differentially expressed in injured/uninjured DRGs after in vivo administration of M1/vehicle for 3 consecutive days (*SI Appendix*, Fig. S4*B*). Similarly, the cytokine expression profiling of injured/uninjured DRGs showed that the protein level of 40 cytokines was not differentially expressed between M1- and vehicle-treated mice 3 d after SNC (*SI Appendix*, Fig. S5). We, therefore, conclude that M1 treatment does not induce or augment inflammatory responses in injured/uninjured mice.

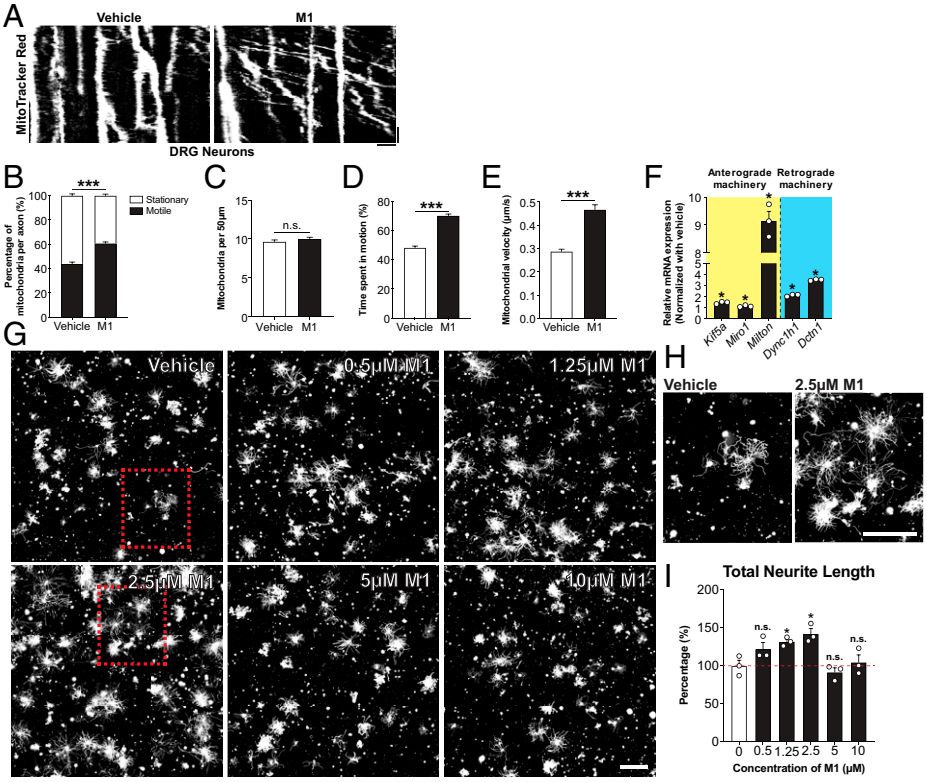

Fig. 2. M1 promotes axonal mitochondrial transport and axon regeneration in cultured adult DRG neurons. (*A*) Representative kymographs of vehicle- (0.1% DMSO) or M1-treated (2.5 μM) adult DRG neurons showing the movement of individual mitochondria (white lines) recorded at one frame per 30 s for 2.5 h. Mitochondrial trafficking was faster in M1-treated than vehicle-treated DRG neurons. Vertical lines represent stationary mitochondria; oblique lines indicate motile mitochondria. A total of 1,198 (vehicle treatment) and 906 (M1 treatment) mitochondrial events were included in the kymograph analysis. (Vertical scale bar: 20 min; horizontal scale bar: 5 μm.) (*B*) M1 treatment increased the motile pool of mitochondria significantly when compared with vehicle control. (*C*) M1 treatment did not alter the mitochondrial density in the 50-μm distal-most axonal segments. (*D*) The moving frequency (indicated by the time each mitochondrion spent in motion) was markedly elevated in M1-treated DRG neurons when compared with vehicle-treated controls. (*E*) The average mitochondrial velocity was increased dramatically after M1 treatment and calculated from the motile pool of mitochondria only. (*F*) M1 treatment up-regulated the mRNA expression of major axonal transport machinery genes (*Kif5a*, *Miro1*, *Milton*, *Dync1h1*, and *Dctn1*) in DRG neurons. Each dot represents the mRNA expression from one independent cell culture experiment. (*G*) Adult DRG neurons were treated with M1 at various concentrations (0.5 to 10 μM), with DMSO (0.1%) serving as the vehicle control. After 17 h of incubation, the neurons were fixed and immunostained with anti–βIII-tubulin antibody for the neurite outgrowth assay. (*H*) Magnified view of the red boxes in *G*. (Scale bars: 500 μm in *G* and *H*.) (*I*) Compared with vehicle-treated controls, the administration of M1 at the 2.5 μM concentration increased maximal neurite outgrowth. Each dot represents the average total neurite outgrowth from one independent cell culture experiment. Adult DRG neurons were prepared from C57BL/6 mice (8 to 12 wk). Data are presented as means ± SEM from six to eight independent experiments in *B*–*E* and as means ± SEM of triplicates in *F* and *I*. The Mann–Whitney *U* test (*B*–*E*), the Student's *t* test (*F*), and one-way ANOVA with Bonferroni's post hoc test (*I*) were used. n.s., not significant. $*P < 0.05$; $***P < 0.001$.

To further verify the in vivo link between mitochondrial dynamics and axon regeneration, we performed ex vivo time-lapse imaging of mitochondria in sciatic nerves. For this, the AAV2/9 serotype vector expressing mitochondrial matrix-targeted green fluorescent protein (mitoGFP; AAV2/9-mitoGFP) was injected into the sciatic nerve of mice to label the mitochondria. Injection was performed 2 wk before M1 treatment and ex vivo time-lapse imaging to allow for sufficient expression and retrograde spread of the green fluorescent protein (GFP) signal (28) (Fig. 3*E*). Consistent with the in vitro results, there was a 22.4% increase in the length of the mitochondria in M1-treated sciatic nerves (1.44 ± 0.02 μm) compared with that for mitochondria in vehicle-treated controls (1.17 ± 0.02 μm) (Fig. 3*F*). M1-treated sciatic nerves also displayed a significantly greater cumulative frequency of larger mitochondria 24 h after M1 administration ($d = 0.082$, $P < 0.01$) (Fig. 3*G*). Notably, ex vivo time-lapse imaging and kymograph analysis suggested that compared with vehicle-treated controls (15.01 ± 2.27%), M1 treatment led to a marked increase in the motile pool of mitochondria (37.78 ± 2.39%) in peripheral axons of the sciatic nerves (Fig. 3 *H* and *I*) without altering the mitochondrial density (Fig. 3*J*). The moving mitochondria from M1-treated sciatic nerves (40.01 ± 1.07%) spent about triple the time in motion relative to those in vehicle-treated sciatic nerves (13.52 ± 0.75%) (Fig. 3*K*). Remarkably, M1 treatment induced a 2.89-fold increase in mitochondrial transport velocity in peripheral axons of the sciatic nerves (1.38 ± 0.04 μm/s in vehicle-treated controls vs. 3.99 ± 0.13 μm/s in M1-treated sciatic nerves) (Fig. 3*L* and Movie S1). Collectively, our results demonstrated the rapid onset of action and therapeutic potential of M1 in axon regeneration in vivo.

M1 Induces Sustained Axon Regeneration in the CNS. To examine if the therapeutic potential of M1 in the PNS could also apply to axon regeneration in the CNS, we first assessed the direct effect of M1 on the extent of neurite outgrowth in primary RGC cultures. The neurite outgrowth assay involved culture of purified postnatal days 1 to 3 mouse RGCs for 3 d followed by automated image analysis (29, 30, 31) (*SI Appendix*, Fig. S6*A*). RGCs treated with M1 (91.94 ± 7.22 μm) exhibited a significant increase in neurite outgrowth with the mean total neurite length per neuron increased to 50% compared with vehicle control (61.46 ± 7.21 μm) (*SI Appendix*, Fig. S6*B*), indicating that M1 is able to induce the intrinsic capacity of RGC to regrow axons.

Next, we tested the promoting effects of M1 on optic nerve regeneration and RGC survival in mice 2 wk after ONC. The mice were treated with M1 or vehicle immediately after ONC by intravitreal injection and then again after 7 d due to a decline in the M1 availability in the retina, as determined by liquid chromatography with tandem mass spectrometry (LC–MS/MS) analysis (*SI Appendix*, Fig. S7*A*). We also compared the effects of M1 treatment with those of knocking down *Pten*, a known RAG (5, 32), to evaluate whether they exerted synergistic effects in promoting axon regeneration in the CNS. Adult *Pten* floxed ($Pten^{fl/fl}$) mice were intravitreally injected once with AAV2-Cre ($Pten^{-/-}$) or AAV2-GFP (control) 2 wk before ONC (Fig. 4*A*). On day 11 post-ONC, mice were intravitreally injected with anterogradely transported CTB to trace regenerating axons; then, the tissue-cleared optic nerve was imaged using confocal microscopy (Fig. 4*B*) (4–6, 33). The loss of *Pten* led to a marked increase in the number of axons (71.3 ± 40.7) growing at 1.5 mm distal from the crush site

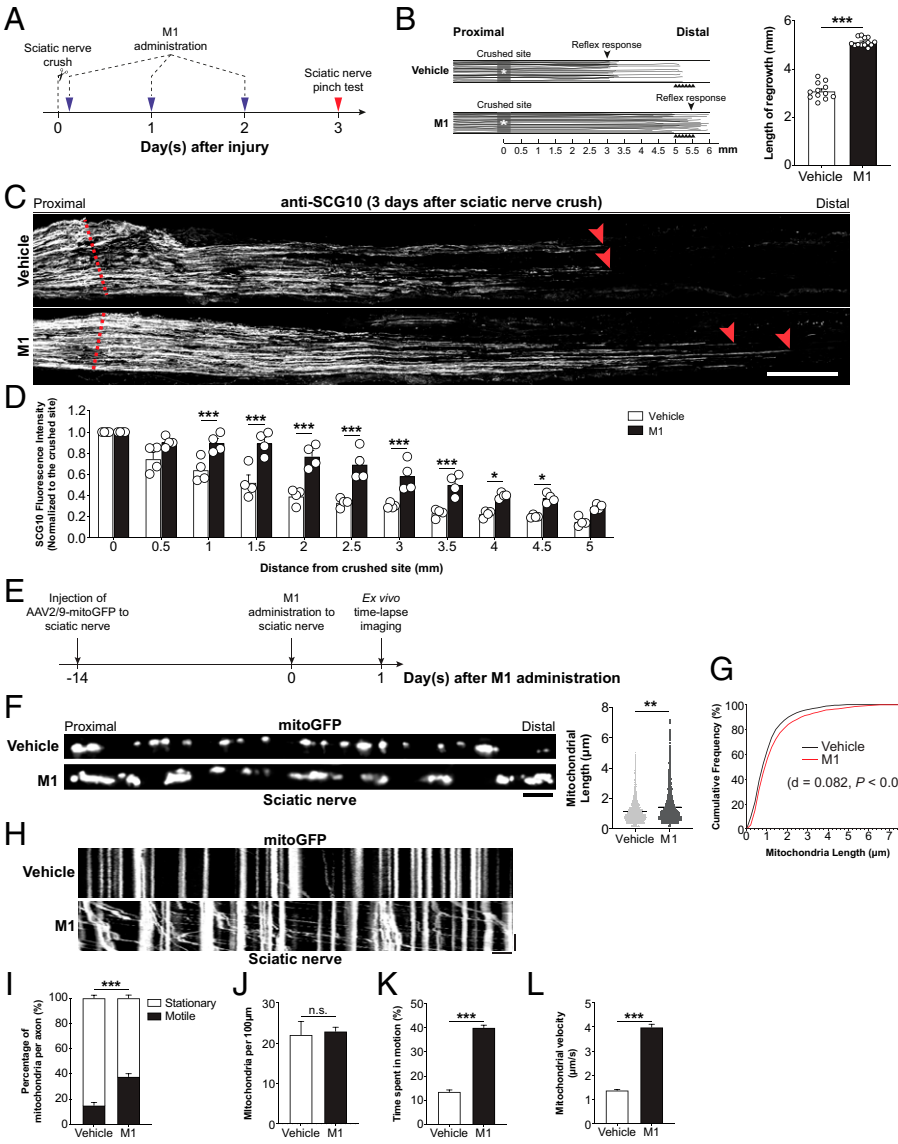

Fig. 3. Peripheral axon regeneration and axonal mitochondrial dynamics are enhanced substantially in M1-treated mice. (*A*) Adult C57BL/6 mice were subjected to SNC, following which 20 μg of M1 was applied to the lesion site immediately after the crush for 3 consecutive days. (*B*) M1 treatment markedly increased the distal extent of axonal regrowth 3 d after injury as determined by the sciatic nerve pinch test (n = 12 for vehicle treatment; n = 13 for M1 treatment). Each dot represents the length of axonal regrowth from one mouse. (*C*) The extent of sensory axonal regrowth was assessed by immunostaining of SCG10 3 d after SNC. SCG10 immunoreactivity was prominent even in the far-distal region of the crushed nerve in the M1-treated mice (red arrowheads). The red dotted line indicates the crush site. (Scale bar: 500 μm.) (*D*) The SCG10 fluorescence intensity was measured in the longitudinal section of the sciatic nerve and normalized to the crush site referred to as the regeneration index (n = 4 per treatment group). Each dot represents the normalized SCG10 fluorescence intensity from one mouse. (*E*) Ex vivo time-lapse imaging of AAV2/9-mitoGFP–labeled mitochondria in sciatic nerves. M1 (20 μg) was applied directly to the sciatic notch, and time-lapse images were captured for kymograph and mitochondrial length analyses 1 d after M1 administration. (*F*) Representative photomicrographs of mitoGFP-labeled mitochondria in sciatic nerves. M1 induced a 22.4% increase in mitochondrial length in the sciatic nerves. A total of 2,390 (vehicle treatment) and 2,053 (M1 treatment) mitochondria from six sciatic nerves per treatment group and three independent experiments were evaluated. (Scale bar: 5 μm.) (*G*) There was a significant increase in the cumulative frequency of larger mitochondria 24 h after M1 treatment. (*H*) Representative kymographs of mitochondrial movement in sciatic nerves of vehicle- and M1-treated mice. The movement of individual mitochondria (white lines) was recorded at one frame per 5 s for 10 min. Vertical lines represent stationary mitochondria, and oblique lines indicate motile mitochondria. M1 markedly accelerated mitochondrial transport in the peripheral axons of sciatic nerves. A total of 1,115 (vehicle treatment) and 1,487 (M1 treatment) mitochondrial events from six sciatic nerves and three independent experiments were included for kymograph analysis. (Vertical scale bar: 200 s; horizontal scale bar: 5 μm.) (*I*) M1 treatment led to a marked increase in motile pool of mitochondria. (*J*) M1 did not affect the mitochondrial density in the 100-μm-long axonal segments in sciatic nerves. (*K*) The moving frequency (indicated by the time each mitochondrion spent in motion) was significantly increased in M1-treated sciatic nerves. (*L*) M1 treatment promoted the average mitochondrial velocity significantly when compared with vehicle controls. Average mitochondrial velocity was calculated from the motile pool of mitochondria only. Data are presented as means ± SEM. The Student's t test (*B*), two-way ANOVA followed by Bonferroni's post hoc test (*D*), the Mann–Whitney U test (*F* and *I*–*L*), and the two-sample Kolmogorov–Smirnov test (*G*) were used. n.s., not significant. *P < 0.05; **P < 0.01; ***P < 0.001.

compared with that in vehicle-treated mice with no axons advanced beyond the crush site, in line with previous reports (6, 32). Regeneration was also enhanced in M1-treated mice, with a significant number of regenerating axons reaching 1.5 mm from the crush site (163.2 ± 49.1). The loss of *Pten* further increased M1-induced axon regeneration, an effect that was most striking for short regenerating axons (Fig. 4*C*). Consistent with that reported in previous studies, RGC survival was reduced to 19% 2 wk after ONC (4, 32, 33); however, following M1 treatment, RGC survival increased to 34.8 ± 2.4% as evidenced by staining for the RNA-binding protein with multiple splicing (RBPMS). A similar extent of neuronal survival was observed with the *Pten*$^{-/-}$ (31.8 ± 0.6%) and *Pten*$^{-/-}$ + M1 treatment (40.4 ± 0.5%) (Fig. 4*D*).

Before we investigate if RGCs can be induced by M1 to regenerate along the entire optic nerve reaching their distant targets, one issue to be addressed is the concerns associated with intraocular inflammation (34, 35). We have carefully examined whether intravitreal injections of M1 or vehicle would trigger microglial activation, infiltration of macrophages/neutrophils, or inflammatory gene and protein expressions in the retinae. The cell numbers as well as the morphology of ionized calcium-binding adapter molecule 1 (IBA-1)–positive microglia remained similar after 14 d of M1 or vehicle treatments in the injured (*SI Appendix*, Fig. S8 *A* and *B*) and uninjured retinae (*SI Appendix*, Fig. S8 *C* and *D*), demonstrating that repeated intravitreal injections of AAV, M1, or vehicle did not further augment microglial activation after ONC. Similarly, we did not observe an increase in the numbers of infiltrating macrophages in the uninjured retinae of M1 or vehicle treatment groups (*SI Appendix*, Fig. S8*E*). We also performed detailed immunohistochemistry analysis in the retina and posterior chamber (vitreous) at the early time points after ONC (days 1 and 3) (*SI Appendix*, Fig. S9*A*), and M1 administration did not augment the infiltration of macrophages/neutrophils into the retina at days 1 and 3 after ONC when compared with the vehicle-treated mice. Additionally, M1 or vehicle

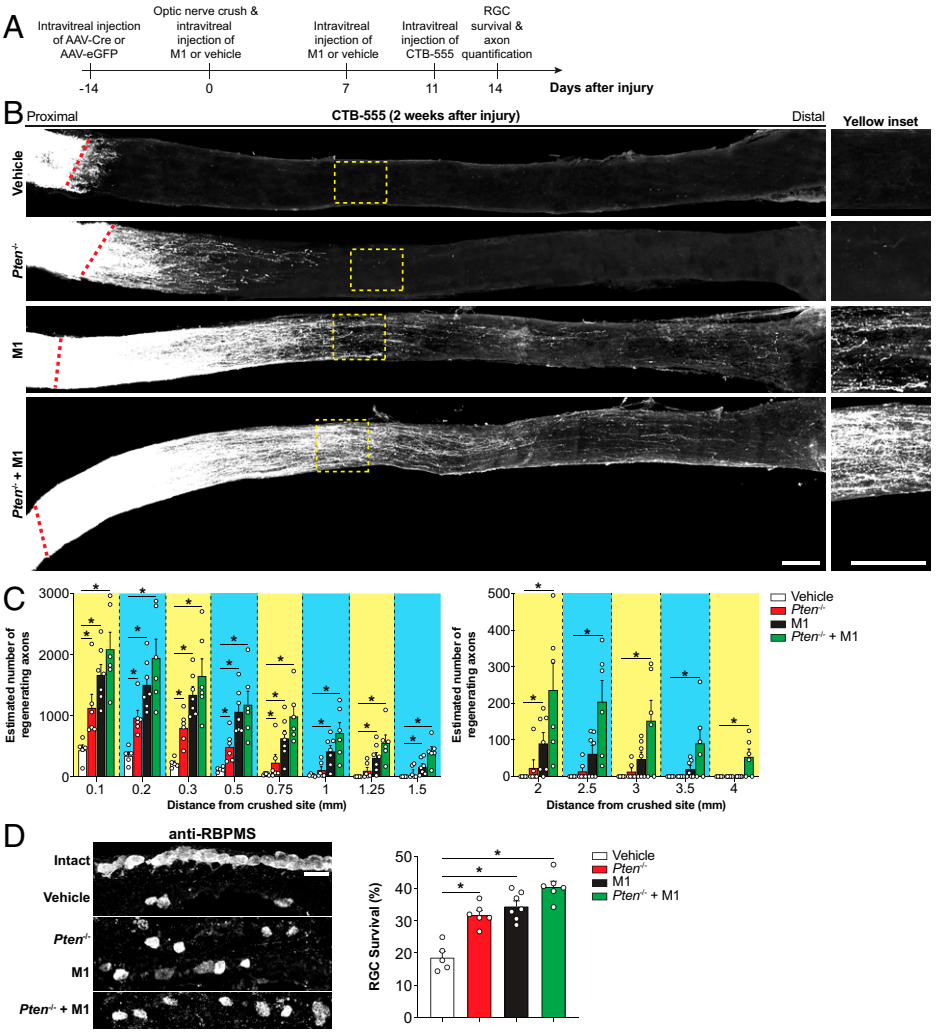

Fig. 4. Intravitreal injection of M1 induces robust axon regeneration 2 wk after ONC. (*A*) Schematic diagram illustrating the M1 (1-μg) treatment paradigm for ONC. *Pten* was knocked down by the intravitreal injection of an AAV2 vector expressing Cre recombinase (AAV2-Cre) in $Pten^{fl/fl}$ mice 2 wk before ONC. AAV2-eGFP served as the control. M1 (1 μg) or vehicle was intravitreally injected into the injured eyes at days 0 and 7 after ONC. Axon regeneration was analyzed by CTB-555 tracing. (*B* and *C*) Compared with that in $Pten^{fl/fl}$ controls, mice treated with M1 displayed long-distance axon regeneration 14 d after ONC, with a significant number of regenerating axons reaching 2 mm from the crush site. *Pten* deletion further increased M1-induced axon regeneration. Red dotted lines indicate the crush sites. Each dot represents the average number of regenerating axons from one mouse. Magnified views of the yellow boxes in *B*, *Left* are shown in *B*, *Right*. (*D*) Over 32% of RGC survival was observed in $Pten^{-/-}$, M1 treatment, and $Pten^{-/-}$ + M1 treatment; however, only ∼20% of RGCs survived in $Pten^{fl/fl}$ control mice 2 wk after ONC injury. Each dot represents the average number of RBPMS-positive RGCs from one mouse. Data are presented as means ± SEM (n = 5 mice for the vehicle-treated group; n = 6 mice for the $Pten^{-/-}$- and $Pten^{-/-}$ + M1–treated groups; n = 7 mice for the M1-treated group). One-way ANOVA followed by Bonferroni's post hoc test was used in *C* and *D*. $^*P < 0.05$. (Scale bars: 200 μm in *B*; 20 μm in *D*.)

administration did not induce infiltrating of macrophages/neutrophils into the posterior chamber of uninjured/injured retinae at days 1 and 3 after ONC (*SI Appendix*, Fig. S9 *B* and *C*). However, intravitreal injection of zymosan (an activator of inflammatory responses) (*SI Appendix*, Fig. S9*D*) led to a massive infiltration of macrophages and neutrophils into the posterior chambers of injured retinae 3 d after ONC (*SI Appendix*, Fig. S9 *E* and *F*) (36, 37). We then determined the gene expression profiles of 14 important inflammatory mediators (*Tnf-α*, *Il-1β*, *Il-6*, *Cd86*, *Nos2*, *Il-4*, *Il-10*, *Cd206*, *Tgf-β*, *Igf-1*, *Ccl2*, *Ccl3*, *Ccl4*, and *Ccl5*) by qPCR. None of these genes were differentially expressed in the naïve (uninjured) mice 14 d after intravitreal injections of M1 or vehicle (*SI Appendix*, Fig. S10*A*). As expected, ONC triggered inflammatory responses and induced up-regulation of the most inflammatory-associated genes (except *Il-4* and *Il-10*) at 14 d post-ONC. However, none of these genes showed differential expression in injured/uninjured retinae of M1/vehicle treatment groups (*SI Appendix*, Fig. S10*B*). On day 14 post-ONC, a cytokine array assay was performed to analyze protein levels of 40 cytokines in M1-/vehicle-treated injured/uninjured retinae (*SI Appendix*, Fig. S11*A*). The inflammatory cytokine profiles remained unchanged after repeated intravitreal injections of M1 or vehicle. We found that ONC induced a similar profile of cytokine production in retinae when treated with M1 or vehicle (*SI Appendix*, Fig. S11*B*). Consistent with previous study, we demonstrated that the intravitreal injection procedure did not trigger inflammation and macrophage infiltration into the retinae (32). Intravitreal injection of M1 did not induce inflammatory responses and altered inflammatory cytokine profiles after ONC. We conclude that M1 did not cause intraocular inflammation in our ONC studies.

To further determine if M1 promotes sustained axon regeneration, we assessed optic nerve regeneration and RGC survival 4 wk after ONC (Fig. 5*A*). In vehicle-treated or $Pten^{-/-}$ mice, virtually no axons were observed 4 mm distal to the crush site. In stark contrast, robust long-distance axon regeneration was observed in M1-treated mice 4 wk after ONC, and some CTB-labeled axons regenerated along the entire length of the optic nerve, even reaching the optic chiasm (Fig. 5*B*). In particular, most optic nerves of M1-treated mice had regenerating axons (156.3 ± 81.2) that reached 4 mm from the crush site, near the optic chiasm, at a much higher level compared with $Pten^{fl/fl}$ vehicle-treated controls and AAV2-Cre–treated ($Pten^{-/-}$) mice in which no regenerating axons were found distally (>4 mm). The regenerating axons of several M1-treated RGCs attained lengths of up to 5 mm (Fig. 5*C*). The actual length of the longest regenerating axons would be more than 5 mm given that the dehydration process during tissue clearing led to optic nerve shrinkage (∼18%) (38). M1 treatment, *Pten* deletion, or a combination of both led to a similar significant increase in RGC survival (32 to 35%) (Fig. 5*D*).

For successful optic nerve regeneration, regenerating RGC axons have to reconnect with their targets in the thalamus, midbrain, and SC (39). Consequently, we investigated whether

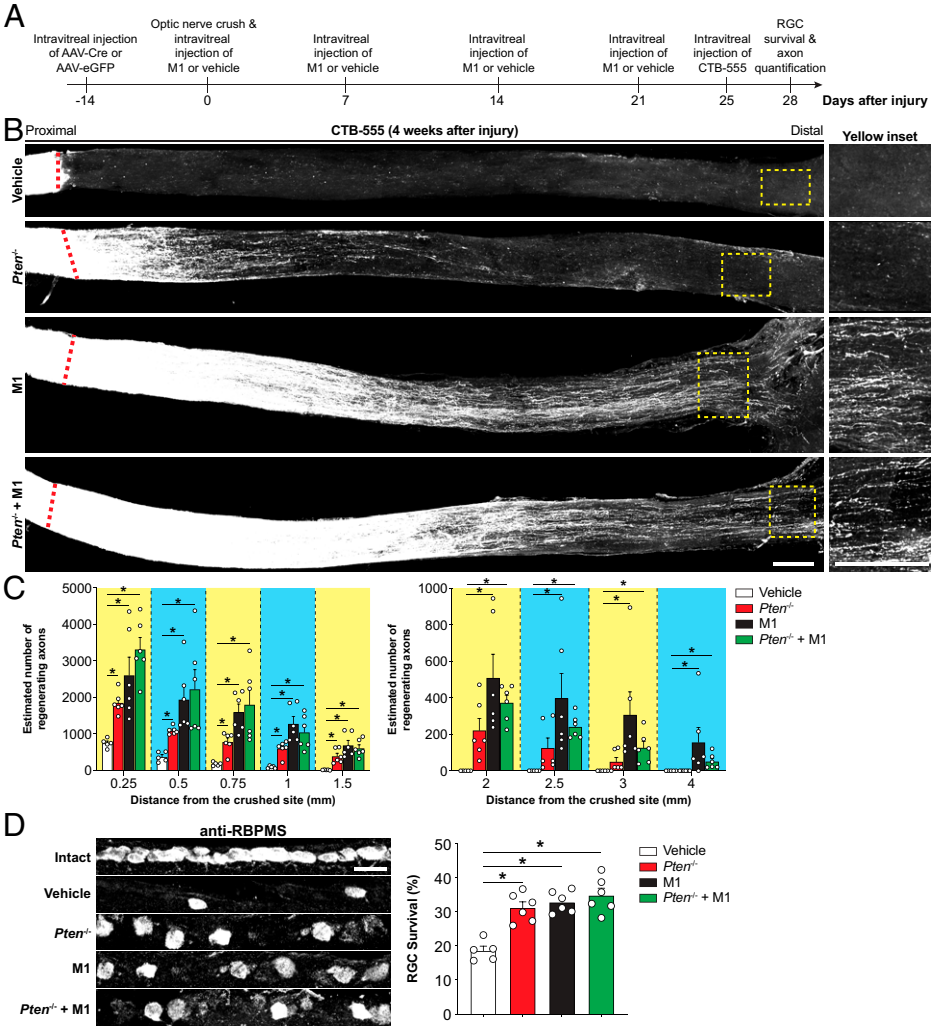

Fig. 5. M1 induces sustained axon regeneration that reaches the optic chiasm 4 wk after ONC. (*A*) Schematic diagram illustrating the M1 (1-μg) treatment paradigm for ONC. *Pten* was knocked down by the intravitreal injection of an AAV2 vector expressing Cre recombinase (AAV2-Cre) in $Pten^{fl/fl}$ mice 2 wk before ONC. AAV2-eGFP served as the control. M1 (1 μg) or vehicle was intravitreally injected into the injured eye at days 0, 7, 14, and 21 after ONC. Axon regeneration was analyzed by CTB tracing (CTB-555). (*B* and *C*) Sustained long-distance axon regeneration was observed in M1-treated mice 4 wk after ONC; some CTB-555–labeled axons regenerated along the entire length of the optic nerve to reach the optic chiasm in M1-treated mice (yellow boxes in *B*). The number of regenerating axons in the combination treatment group ($Pten^{-/-}$ + M1) was comparable with that of M1-treated mice, indicating that M1 alone is sufficient to induce sustained axon regeneration. Red dotted lines indicate the crush sites. Each dot represents the average number of regenerating axons from one mouse. Magnified views of the yellow boxes in *B*, *Left* are shown in *B*, *Right*. (*D*) M1 treatment, *Pten* deletion, or a combination of *Pten* deletion and M1 administration led to a similar significant increase in RGC survival. M1 treatment did not further enhance RGC survival in $Pten^{-/-}$ mice. Each dot represents the average number of RBPMS-positive RGCs from one mouse. Data are presented as means ± SEM (n = 5 mice for the vehicle-treated group; n = 6 mice for the $Pten^{-/-}$-, M1-, and $Pten^{-/-}$ + M1–treated groups). One-way ANOVA followed by Bonferroni's post hoc test was used in *C* and *D*. *$P < 0.05$. (Scale bars: 200 μm in *B*; 20 μm in *D*.)

M1 treatment is sufficient to sustain long-distance axon growth by tracing regenerating axon projections from the optic chiasm to multiple subcortical visual targets at 6 wk post-ONC (Fig. 6*A*). M1 treatment resulted in substantial axon regeneration, with many CTB-positive RGC axons entering and crossing the hypothalamic suprachiasmatic nucleus (SCN) (Fig. 6*B*), extending distally into the optic tract ∼1 mm caudal to the optic chiasm (Fig. 6*C*), and reaching the ventral lateral geniculate nucleus (vLGN) (Fig. 6*D*) and the dorsal lateral geniculate nucleus (dLGN) (Fig. 6*E*) in the thalamus. Notably, a considerable number of regenerating axons grew into the olivary pretectal nucleus (OPN) in the midbrain (Fig. 6*F*), while some even reached the brachium and the zonal layer of the SC (the site of recording electrode placement; see below) for target reinnervation (Fig. 6*G*). Quantitative analysis of the fluorescent intensity of CTB-labeled regenerating axons was performed, and reinnervation of multiple visual targets was evidenced by substantial CTB-labeled regenerating RGC axons in the M1 and $Pten^{-/-}$ + M1 treatment groups at 6 wk post-ONC (Fig. 6*H*). In contrast, no CTB-labeled regenerating RGC axons were detected in the same subcortical visual target areas of vehicle-treated mice (*SI Appendix*, Fig. S12).

To rule out the possibility that the CTB-positive RGC axons were observed in the optic nerve and multiple visual targets were spared RGC axons and not regenerated axons, mice were intravitreally injected with recombinant CTB conjugated to Alexa Fluor 488 (CTB-488) into the left eye to label intact RGC axons 2 d before ONC. Immediately after the ONC procedure, M1 was administered to the injured (left) eye by intravitreal injection. To anterogradely label the regenerating RGC axons, CTB-555 was intravitreally injected 1 d after ONC, and the optic nerve was harvested 2 d later for imaging (*SI Appendix*, Fig. S13*A*). Three days after ONC and M1 administration, CTB-488–positive axons were observed only at the proximal portions of the optic nerve but never distal to the crush site, indicating the absence of axon sparing. In the same mice, regenerating axons labeled with CTB-555 extended through and beyond the crush site. There was no overlap between CTB-488 (intact uninjured axons) and CTB-555 (regenerating axons) fluorescence in the crushed optic nerve distal to the crush site (*SI Appendix*, Fig. S13*B*). In the uninjured optic nerves, nonlesioned axons were effectively labeled by anterograde CTB-488 (*SI Appendix*, Fig. S13*C*). We, therefore, conclude that the ONC procedure was completed and did not spare RGC axons.

Long-Distance Regenerated Axons Elicit Neural Activities in Target Brain Regions and Restore PLR and Responses to Looming Visual Stimuli. Next, we questioned whether the regenerating axons that had reached their targets could restore neural activity and visual function after injury. To address this, we first performed LFP recordings in the SC following optogenetic activation of channel rhodopsin-2 (ChR2)–transduced RGCs 6 wk after ONC. An AAV vector expressing a ChR2-mCherry fusion protein was intravitreally injected into the injured eye 2 wk before the LFP recording (Fig. 7*A*). To enhance

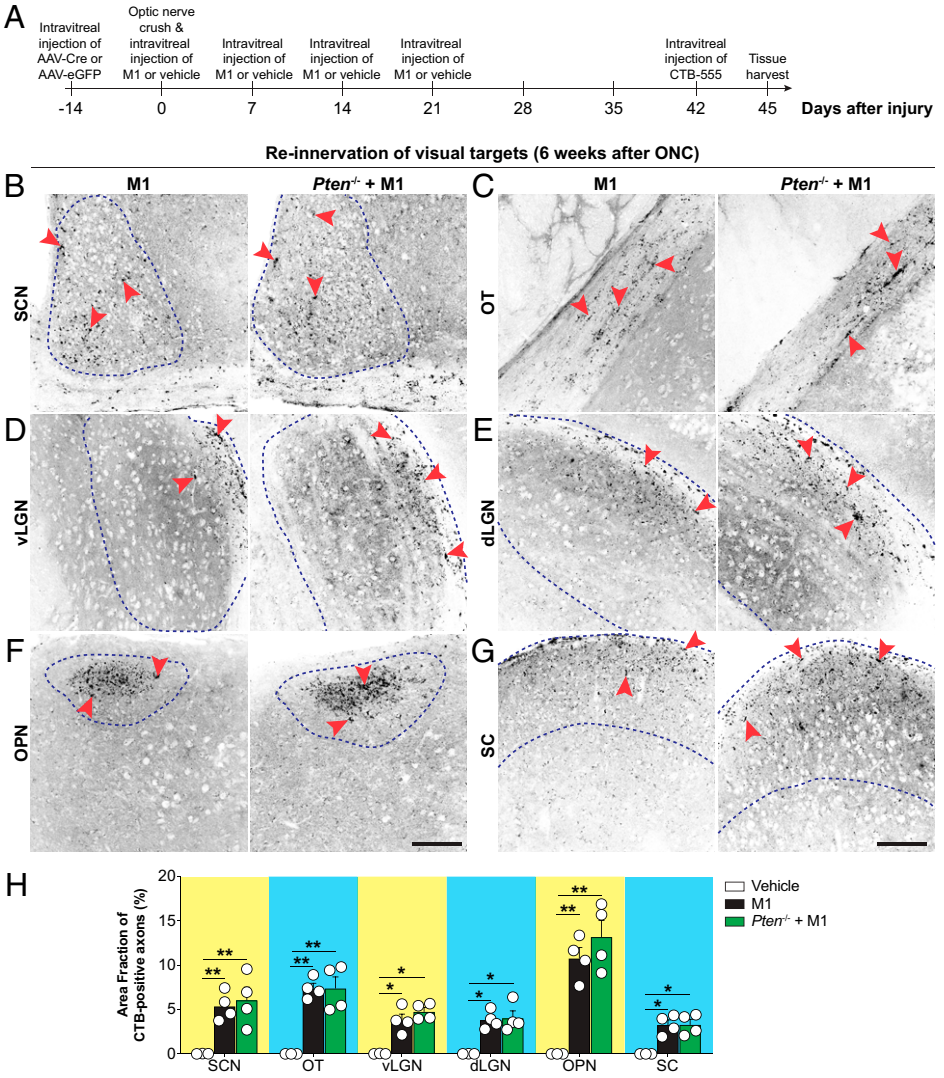

Fig. 6. Regenerating RGC axons reinnervate multiple subcortical visual targets 6 wk after M1 treatment. (*A*) Schematic diagram illustrating the M1 (1-μg) treatment paradigm for ONC. *Pten* was knocked down by the intravitreal injection of an AAV2 vector expressing Cre recombinase (AAV2-Cre) in $Pten^{fl/fl}$ mice 2 wk before ONC. AAV2-eGFP served as the control. M1 (1 μg) or vehicle was intravitreally injected into the injured eyes at days 0, 7, 14, and 21 after ONC. Axon regeneration was analyzed by CTB tracing (CTB-555). (*B*–*G*) Representative confocal micrographs of coronal brain sections showed that a considerable number of CTB-555–positive regenerating RGC axons (red arrowheads) was observed in the (*B*) hypothalamic SCN, (*C*) optic tract (OT), (*D*) thalamic vLGN, (*E*) dLGN, (*F*) OPN, and (*G*) SC of both M1- and $Pten^{-/-}$ + M1–treated mice at 6 wk post-ONC. (Scale bars: 50 μm.) (*H*) Quantification of the area fraction of CTB-positive axons revealed that both M1-treated and $Pten^{-/-}$ + M1–treated mice exhibited a significant number of regenerating axons that reinnervated into different subcortical visual targets at 6 wk post-ONC. Each dot represents the area fraction of CTB-positive axons from one mouse. Data are presented as means ± SEM (n = 3 mice for the vehicle-treated group; n = 4 mice for the M1- and $Pten^{-/-}$ + M1–treated groups). One-way ANOVA followed by Bonferroni's post hoc test was used. *$P < 0.05$; **$P < 0.01$.

the conduction of regenerating axons, 4-aminopyridine (4-AP), a Food and Drug Administration–approved voltage-gated potassium channel blocker, was intraperitoneally injected 3 h before the recordings were initiated (40). We recorded evoked LFPs in response to focal laser stimulation of ChR2-transduced RGCs in the SC and selected the evoked LFPs that were at least twice the recorded baseline LFP for analysis. Over 200 events per animal were averaged in synchrony with optogenetic stimulation to generate the LFP waveform. In uninjured eyes, we could reliably record eye-evoked LFPs from the SC induced by optogenetic activation of ChR2-mCherry–transduced RGCs 2 wk after AAV2-ChR2-mCherry injection. The obtained LFP value (372 ± 54.28 μV) was comparable with that reported in a previous study (40). In contrast, only minimal eye-evoked LFPs were recorded from the SC (13.8 ± 1.6 μV) in vehicle-treated mice 6 wk after ONC. Strikingly, M1 treatment led to a sixfold increase in the maximal amplitude of eye-evoked LFPs (82.1 ± 5.1 μV). The combination treatment (AAV2-Cre [$Pten^{-/-}$] + M1) further increased the eye-evoked LFPs to 97.2 ± 3.7 μV (Fig. 7 *B* and *C*).

To investigate if these substantial restorations of neural activity in the OPN and SC were sufficient to restore visual function, we first performed a PLR test (41) 6 wk after ONC. Mice were treated with 4-AP 3 h before visual function tests and dark adapted for 1 h to achieve full pupil dilation. Then, the lesioned eyes were illuminated with blue light at the 470-nm wavelength (Fig. 7*D*), and the average change in pupil area following illumination was quantified (Fig. 7*E*). In nonlesioned eyes, light stimulation decreased the pupil area by 73.5 ± 3.2%, while the vehicle-treated mice were unable to constrict fully, and pupil constriction was reduced to 27.1 ± 4.6% of the pupil area following light stimulation. Notably, no significant difference in percentage change in the pupil area was found among nonlesioned eyes, M1-treated lesioned eyes, and $Pten^{-/-}$ + M1–treated lesioned eyes, indicating that M1 treatment alone can rescue the pupil constriction response after ONC (Fig. 7*F*). These results are in line with our histology studies that M1-treated RGCs project axons into the SCN (Fig. 6*B*) and OPN (Fig. 6*F*), which are the main regions in the brain that control the PLR (42).

Next, we assessed the responses of the mice to a looming visual stimulus, a behavior mainly driven via long-distance RGC projections to the SC (43, 44). We placed each mouse into an open Plexiglas chamber equipped with a triangular prism–shaped shelter. Freezing and escape can be reliably triggered by an overhead display of a rapidly expanding black circle. Each mouse received an eyelid suture in the nonlesion eye to eliminate vision through the intact eye. As expected, uninjured mice with normal vision immediately froze and ran under the shelter upon presentation of the looming stimulus.

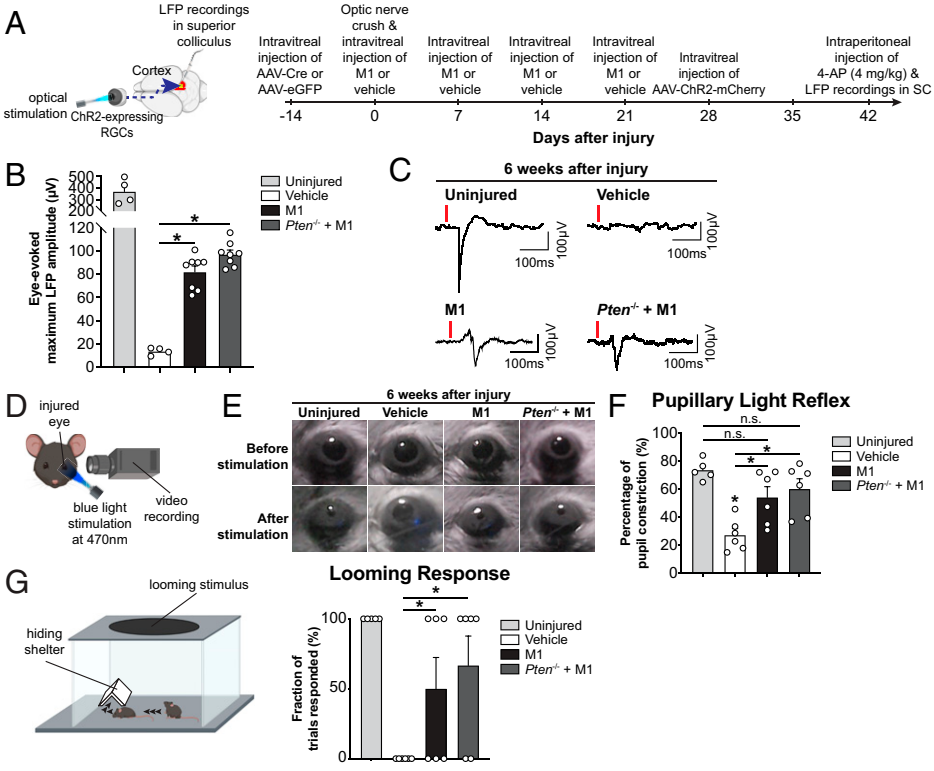

Fig. 7. Long-distance regenerated axons elicit neural activity in target brain regions to restore the PLR and responses to looming visual stimuli. (*A*) Schematic diagram illustrating the M1 (1-μg) treatment paradigm for ONC and LFP recording in the SC upon optogenetic stimulation of RGCs. M1 (1 μg) or vehicle was intravitreally injected into the injured eye at days 0, 7, 14, and 21 after ONC. Adult mice were administered AAV2-ChR2-mCherry by intravitreal injection at day 28 post-ONC. LFPs were evoked in the SC by the focal laser stimulation of ChR2-expressing RGCs at day 42 post-ONC. (*B*) Eye-evoked LFP amplitudes were determined using Spike2 software and a customized MATLAB program. M1 administration led to a marked increase in eye-evoked LFP amplitudes compared with vehicle-treated controls. The combination of *Pten*$^{-/-}$ + M1 treatment further augmented the M1-induced increase in LFP amplitudes after the optogenetic stimulation of injured RGCs; in contrast, only minimal eye-evoked LFPs were recorded from the SCs of vehicle-treated mice 6 wk after ONC (n = 4 mice for the uninjured and vehicle-treated groups; n = 8 mice for M1- and *Pten*$^{-/-}$ + M1–treated groups). Each dot represents the average eye-evoked LFP amplitude from one mouse. (*C*) Representative eye-evoked LFPs for all the treatment groups. Red lines indicate optogenetic stimulation in the injured eye. (*D*) Schematic diagram illustrating the PLR test. Mice were dark adapted for 1 h before the PLR test. The relative pupil constriction was calculated as the percentage change in pupil area between the baseline reading after 1 h of dark adaptation and the reading obtained after 30 s of light stimulation (30 lx) at 470 nm. (*E*) Representative images of the PLR from vehicle-treated control, M1-treated, and *Pten*$^{-/-}$ + M1–treated mice. (*F*) The vehicle-treated pupils of control mice failed to fully constrict upon light stimulus. Pupil constriction was restored to baseline levels in both M1- and *Pten*$^{-/-}$ + M1–treated mice (n = 4 mice for the uninjured group; n = 6 mice for the vehicle-, M1-, and *Pten*$^{-/-}$ + M1–treated groups). Each dot represents the pupil constriction from one mouse. (*G*) Uninjured mice with normal vision immediately froze and ran under the shelter following looming visual stimulation. In contrast, none of the vehicle-treated lesioned mice responded to the looming stimulus. Half of the M1-treated mice responded to the looming stimulus by hiding in the shelter (n = 6 mice per treatment group). Each dot represents the looming response from one mouse. Data are presented as means ± SEM. One-way ANOVA with Bonferroni's post hoc test was used. n.s., not significant. *P < 0.05.

In contrast, these visually evoked defensive responses were completely lost in vehicle-treated mice 6 wk post-ONC.

Strikingly, in the M1 and *Pten*$^{-/-}$ + M1 treatment groups, 50 and 67% of the mice, respectively, responded to the looming stimulus by hiding in the shelter (Fig. 7*G* and Movie S2). At an early time point (4 wk post-ONC) (*SI Appendix*, Fig. S14*A*), an improvement in neural activity (*SI Appendix*, Fig. S14 *B* and *C*) and PLR was observed in M1- and *Pten*$^{-/-}$ + M1–treated mice (*SI Appendix*, Fig. S14 *D–F*), whereas none of the lesioned mice responded to the looming stimulus. These results collectively suggested that M1 induces sustained and long-distance axon regeneration, which then promotes reinnervation of the SC, a multisensory midbrain structure that integrates visual, auditory, and somatosensory spatial information to initiate motor movement and coordination (43, 44).

The Essential Role of Mitochondrial Dynamics in CNS Axon Regeneration. Growing evidence suggests that mitochondrial dynamics is a critical determinant of successful regeneration, especially during the active growth phase of axon regeneration (6, 10, 45). Our data showed that M1 enhanced axonal mitochondrial fusion, transport, and movement in neurons. To gain further insight into the critical roles of mitochondrial dynamics in the CNS regeneration, we first assessed how M1 treatment affected the mRNA expression of key genes encoding mitochondrial fusion proteins (*Opa1* and *Mfn2*) and major axonal transport machinery proteins (*Kif5a*, *Miro1*, *Milton*, *Dync1h1*, and *Dctn1*) in the retina. We found that all were up-regulated following M1 treatment (*SI Appendix*, Fig. S15 *A* and *B*). Subsequently, we silenced *Mfn2* or *Opa1* expression in retinae of M1-treated mice after ONC via the intravitreal injection of AAV2 vectors expressing short hairpin RNA (shRNA) targeting *Opa1* (AAV2-*Opa1*-shRNA) or *Mfn2* (AAV2-*Mfn2*-shRNA) 2 wk before ONC (Fig. 8*A*). Consistent with previous studies (5, 32, 46), intravitreal injection of AAV2-mediated shRNA [tagged with enhanced green fluorescent protein; (eGFP)] (*SI Appendix*, Fig. S15*C*) preferentially targeted RGCs as indicated by the high percentage of cells in the ganglion cell layer, which were both GFP positive and βIII-tubulin positive (neuronal marker) (*SI Appendix*, Fig. S15*D*). Endogenous OPA1 and MFN2 were ubiquitously expressed in the RGC layer, but very low expressions of OPA1 and MFN2 were observed in the other cell layers, and they were undetectable in the rod/cone cells in the inner/outer segments (*SI Appendix*, Fig. S15 *E* and *F*). The intravitreal administration of AAV2-*Opa1*-shRNA and AAV2-*Mfn2*-shRNA markedly reduced the retinal mRNA levels of *Opa1* (87.1% reduction) and *Mfn2* (84.0% reduction), respectively (*SI Appendix*, Fig. S15 *G* and *H*). Notably, the growth-promoting effect of M1 was completely abolished following the knockdown of either gene. There were virtually no CTB-positive regenerating axons observed following AAV2-*Opa1*-shRNA + M1 and AAV2-*Mfn2*-shRNA + M1 treatment (Fig. 8*B*), indicating that high expression levels of *Opa1* or *Mfn2* are required for the successful optic nerve regeneration. Consistent with our results, AAV2-scr-shRNA (scramble shRNA control) + M1 treatment induced over 176 axons regenerated 2 mm beyond the crush site (Fig. 8*C*). The protective effect of M1 on RGC survival was also abolished after *Mfn2 or Opa1* knockdown (Fig. 8*D*). These findings exemplify the importance of mitochondria-based

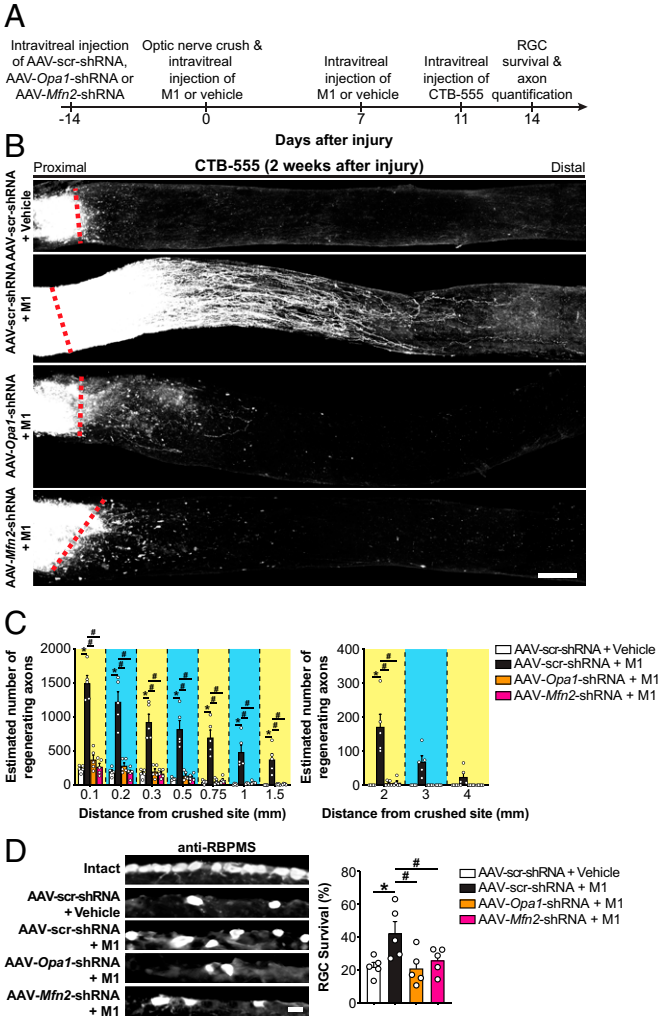

Fig. 8. The knockdown of genes encoding mitochondrial fusion proteins abolished M1-induced optic nerve regeneration. (*A*) In vivo AAV2-mediated silencing of the *Opa1* or *Mfn2* genes in retinae of M1-treated mice by the intravitreal injection of AAV2 vectors expressing shRNAs 2 wk before ONC. AAV2-scramble (AAV2-scr-shRNA) was used as a control. M1 (1 μg) or vehicle was intravitreally injected into the injured eye at days 0 and 7 after ONC. Three days before tissue harvesting, mice were intravitreally injected with 2 μg of CTB-555 to trace regenerating axons. (*B* and *C*) M1 treatment induced robust axon regeneration 14 d after ONC; however, this effect was abolished following the knockdown of either *Opa1* or *Mfn2*, suggesting that the regeneration-promoting effects of M1 in the optic nerve were mediated through the activation of mitochondrial fusion. Red dotted lines indicates the crush sites. Each dot represents the average number of regenerating axons from one mouse. (*D*) The protective effect of M1 on RGC survival was also abolished after *Mfn2 or Opa1* knockdown. Each dot represents the average number of RBPMS-positive RGCs from one mouse. Data are presented as means ± SEM ($n = 5$ per group). One-way ANOVA followed by Bonferroni's post hoc test was used in *C* and *D*. $^{*}P < 0.05$ compared with AAV2-scr-shRNA + vehicle controls; $^{\#}P < 0.05$ compared with the AAV2-scr-shRNA + M1 treatment group. (Scale bars: 200 μm in *B*; 20 μm in *D*.)

approaches in enhancing axon regeneration and functional recovery after CNS injury.

Discussion

Long-distance axon regeneration and meaningful functional recovery are virtually nonexistent in the adult mammalian CNS and are also highly challenging therapeutic goals. The combined expression of RAGs is known to facilitate axon regeneration and promote recovery of neural activity in target brain regions, but function recovery remains difficult to achieve (4–6, 40). In young CNS neurons, mitochondria are highly mobile and are transported bidirectionally along axons to meet the high energy demands of the growing cells; however, this mitochondrial dynamics along with intrinsic regenerative capacity decreases as neurons mature (47). Mitochondrial dynamics often refers to a broad spectrum of features, such as mitochondrial fission–fusion, movement, and transport. Our study revealed that a single small molecule, M1, could enhance mitochondrial dynamics by increasing mitochondrial length, motility, and transport velocity such that axon regeneration would become possible in the hostile environment that is the CNS.

Mitochondria are the powerhouses of cells, and mitochondrial dynamics are essential for neuronal growth, survival, function, and axon regeneration after injury. A large body of evidence supports that mitochondrial dysfunction may be a major contributing factor in many neurodegenerative diseases; accordingly, mitochondria are also important therapeutic targets for the treatment of nervous system injury (6, 10, 11, 15,48). Mitochondrial fusion involves the merging of two mitochondria into one through an end-to-end collision and is tightly orchestrated by three GTPase proteins: MFN1 and MFN2 for the fusion of the mitochondrial outer membrane followed by OPA1 for the fusion of the mitochondrial inner membrane (48). Growing evidence suggests that the two processes, fission–fusion and axonal mitochondrial transport, are not necessarily an interdependent process. For instance, knockdown of mitochondrial fusion protein MFN2 or OPA1 or overexpression of the Charcot-Marie-Tooth disease type 2A (CMT2A)-causing mutant MFN2-R94Q led to a marked reduction in mitochondrial size (due to an increase in mitochondrial fragmentation), in which the mitochondrial transport velocity was subsequently reduced in cultured DRG neurons, possibly due to the loss of interaction between MFN2 and the Miro/Milton complex (49). MFN2 formed the complex with the outer membrane protein Miro to facilitate proper axonal mitochondrial transport (49, 50). Restoring proper expression of mitochondrial fusion by overexpressing MFN1 rescued the axonal mitochondrial transport defects in DRG neurons lacking MFN2 expression. Knockdown of *Opa1* severely disrupted the axonal mitochondrial fusion in DRG neurons; however, the axonal mitochondrial transport in *Opa1* knockdown DRG neurons was unaffected (49). Indeed, large and elongated mitochondria often exhibit a higher calcium-buffering capacity and elevated adenosine triphosphate (ATP) production, which protected them from mitophagy under stress conditions, such as neuronal injuries (48).

M1 was identified as a "promoter" of mitochondrial fusion in a large-scale screen of 75,000 commercially available small molecules in mouse embryonic fibroblasts (MEFs) (19). The knockout of the *Mfn1 or Mfn2* genes, which encode mitochondrial fusion proteins, results in mitochondrial fragmentation and early signs of apoptosis; however, these effects can be rescued by M1 treatment in cultures of $Mfn1^{-/-}$ or $Mfn2^{-/-}$ MEFs. The administration of M1 in MEFs results in larger mitochondria but does not affect endoplasmic reticulum or lysosome morphology, suggesting that M1 acts in a mitochondria-specific manner and may have high therapeutic value. In rats, M1 can restore OPA1 protein expression levels and ATP levels along with an increase in the activities of mitochondrial complexes I, IV, and V in diabetic hearts (51). Similarly, M1 treatment restored basal expression levels of several mitochondrial fusion–fission proteins (MFN1, MFN2 [mitochondrial fusion], FIS1, and DRP1 [mitochondrial fission]) in neuronal PC12 cells treated with polybrominated diphenyl ethers (PBDEs), a chemical agent that disrupts

mitochondrial homeostasis by significantly reducing the expression levels of proteins involved in mitochondrial fusion and fission. Importantly, M1 treatment also rescued ATP production and the mitochondria fragmentation phenotype in PBDE-treated PC12 cells (52). Injury to the CNS, such as traumatic brain injury and spinal cord injury, acutely impairs axonal mitochondrial transport and triggers a local energy deficit in injured axons (7, 53, 54). Therapeutic interventions that aim to promote axonal mitochondrial transport, including genetic ablation of *snph* and overexpression of armadillo repeat-containing X-linked 1 (*Armcx1*) or Miro1, induce robust axonal regrowth after injury (6, 7, 10, 16). Axon regeneration is a highly energy-demanding process, suggesting that enhancing axonal mitochondrial transport could be a way to accelerate the redistribution of healthy mitochondria toward the active growing regenerating axons where actin polymerization occurs (11) and the active removal of injury-induced damaged mitochondria. To this end, we speculate that the beneficial effects of M1 treatment are not limited to the promotion of mitochondrial fusion but also involve the increase of mitochondrial transport motility and velocity in the regenerating axons (6, 16). The precise mechanism of M1 in promoting axon regeneration may warrant further investigation.

The restoration of visual functions and vision-related behaviors, such as the PLR and responses to looming visual stimuli, depends both on long-distance axon regeneration and on reinnervation of visual targets in the brain. After ONC, the number of regenerating axons in the combination treatment group ($Pten^{-/-}$ + M1) was comparable with that of M1-treated mice, indicating that M1 alone is sufficient to induce sustained axon regeneration. However, such a long-distance axon regeneration induced by a single gene or molecule within 4 wk after optic nerve injury, to our knowledge, has not been reported previously. For instance, although the overexpression of ciliary neurotrophic factor (CNTF) alone induced axon regeneration up to 2 mm distal to the crush site 6 wk after ONC, none of the regenerating axons reached the optic chiasm. Similarly, the overexpression of the RNA-binding protein Lin28a was shown to promote axonal regrowth up to 2 mm distal to the crush site 4 wk after ONC (38), but only a handful of regenerating axons reached the optic chiasm in Lin28a-overexpressing mice 6 wk after ONC (55). Combinatorial treatments for CNS axon regeneration, which target several mechanisms that normally inhibit axonal regrowth, would facilitate robust axon regeneration results in visual function recovery. The coablation of *Pten* and *Socs3* (together with CNTF overexpression) not only induced axon regenerating into the SCN at 4 to 12 wk post-ONC (5, 56, 57) but also, increased mitochondrial density and axonal mitochondrial transport in cultured cortical neurons (58). Bioinformatics analysis revealed that an integral mitochondrial membrane protein, *Armcx1*, was significantly up-regulated in RGCs of *Pten*/*Socs3* double-knockout mice after injury. The overexpression of *Armcx1* alone or in $Pten^{-/-}$ mice increased mitochondrial motility and density while also promoting axon regeneration to a certain extent, indicating a synergistic effect with *Pten* knockout (6). An optic tract transection proximal to the SC led to a significant loss in eye-evoked LFP amplitudes; however, *Pten* and *Socs3* codeletion or co-overexpression of osteopontin, insulin-like growth factor 1, and CNTF induced robust axon regeneration to reinnervate SC, leading to a partial restoration of eye-evoked LFP amplitudes at 6 to 8 wk after optic tract transection. By enhancing the nerve conduction of regenerating axons using 4-AP, the optomotor responses were partially restored in *Pten*/*Socs3*-codeleted mice (40). Combining genetic ablation of *Pten*, zymosan, and cyclic adenosine monophosphate (cAMP) enabled axon regeneration through the entire length of optic nerve, which continued to grow across the optic chiasm and reached the vLGN at 6 wk post-ONC (35). A follow-up study revealed that some of the axons could regenerate more distally to reach OPN, the medial terminal nucleus (MTN), and SC at 10 wk after ONC, leading to a partial restoration of visual-guided behaviors, such as optomotor responses and visual cliff (34). In another study, combining overexpression of cRheb1 (positive regulation of the mTOR signaling pathway) and visual stimulation successfully sustained axonal regrowth to reconnect multiple subcortical visual targets, including SCN, vLGN, dLGN, OPN, MTN, and SC, at 3 wk post-ONC, resulting in partial restoration of optokinetic reflex and defensive responses to looming visual stimuli (59).

In the current study, we showed that M1 increased axonal regrowth into the OPN and completely restored the PLR after ONC. The OPN is a key midbrain structure that modulates the PLR via direct input from intrinsically photosensitive retinal ganglion cells (ipRGCs) (42). The OPN receives overlapping ipRGC and conventional RGC innervation, suggesting that both RGC subtypes are likely to also play a role in visual behaviors other than the PLR (42, 60). The results of these studies give rise to the expectation that M1 induces substantial ipRGC axon regeneration and OPN reinnervation, resulting in the complete recovery of the PLR after ONC. The response to looming visual stimulation probes the retino-subcortical pathways (retinotectal connection) (43, 44), which agreed well with our histology study showing significant regeneration of RGC axons into the SC. In the combination treatment group ($Pten^{-/-}$ + M1), the number of regenerating RGC axons reaching the optic chiasm was comparable with that in the M1-only treatment group. The RGC subtype specificity for responses to looming visual stimuli remains poorly understood, despite a recent study implicating a subset of α-RGCs as indispensable for looming-triggered innate defensive response (61). α-RGCs preferentially regenerate following *Pten* deletion, which supports a combination treatment strategy for optic nerve injury, in which the restoration of neural pathways for visual function requires the regeneration of axons from diverse RGC subtypes. Overall, these studies suggest that M1 treatment imparts unprecedented regenerative capacity to injured neurons and supports the notion that M1 has high therapeutic potential for CNS nerve repair. Therefore, further investigation is warranted to evaluate the clinical application of M1.

In conclusion, we have shown that M1 administration may represent a viable, nonviral therapeutic strategy for the treatment of optic nerve injuries. Several clinical studies have demonstrated the feasibility of using intravitreal administration of drugs or stem cells to treat patients with neovascular age-related macular degeneration and retinitis pigmentosa (62, 63). The potential clinical use of M1 will require lengthy clinical trials. Nevertheless, novel drugs for nervous system repair are urgently needed. To this end, clinically approved mitochondria-modulating drugs can be repurposed to treat nervous system injuries that require further investigation.

Materials and Methods

All experiments were performed according to published methods. Details of the methods are included in *SI Appendix*. The detailed methods included in *SI Appendix* are the animals; primary culture of DRG neurons; live-cell imaging for kymograph analysis; quantification of mitochondrial size in DRG neurons; ex vivo time-lapse imaging of mitochondria in the sciatic nerve; localization of OPA1 and MFN2 in cultured DRG neurons; RNA extraction and real-time qPCR analysis;

subcellular fractionation and western blot analysis; neurite outgrowth and survival assay; SNC and nerve pinch test; quantification of regenerating axons; characterization of immune cell profiles in DRGs and sciatic nerves; mouse cytokine array analysis; primary RGC cultures; ONC, M1 treatment, and AAV administration; detection of M1 in the whole retinae by HPLC–MS/MS analysis; axon quantification and RGC survival assay; characterization of immune cells in the retina and posterior chamber; detection of microglial activation and macrophage infiltration in retinae; optogenetic stimulation of RGCs, LFP recordings, and axon regeneration in the SC; the PLR test; the looming visual stimulus behavioral test; and statistical analysis.

Data, Materials, and Code Availability. All study data are included in the article and/or supporting information.

ACKNOWLEDGMENTS. We thank Prof. Markus Meister of the California Institute of Technology for providing the code for the looming visual stimulus test. This work was supported in part by a General Research Fund from Research Grant Council of the Government of the Hong Kong Special Administrative Region Grants CityU 11100519 and CityU 11100318 and Health and Medical Research Fund, Food and Health Bureau, Hong Kong Special Administrative Region Government Grant 07181356 (to C.H.E.M.).

Author affiliations: [a]Department of Neuroscience, City University of Hong Kong, Hong Kong Special Administrative Region (HKSAR), China; and [b]Department of Chemistry, City University of Hong Kong, Hong Kong Special Administrative Region (HKSAR), China

1. B. T. Lang *et al.*, Pleiotropic molecules in axon regeneration and neuroinflammation. *Exp. Neurol.* **258**, 17–23 (2014).
2. J. E. Kim, B. P. Liu, J. H. Park, S. M. Strittmatter, Nogo-66 receptor prevents raphespinal and rubrospinal axon regeneration and limits functional recovery from spinal cord injury. *Neuron* **44**, 439–451 (2004).
3. B. Zheng *et al.*, Genetic deletion of the Nogo receptor does not reduce neurite inhibition in vitro or promote corticospinal tract regeneration in vivo. *Proc. Natl. Acad. Sci. U.S.A.* **102**, 1205–1210 (2005).
4. P. D. Smith *et al.*, SOCS3 deletion promotes optic nerve regeneration in vivo. *Neuron* **64**, 617–623 (2009).
5. F. Sun *et al.*, Sustained axon regeneration induced by co-deletion of PTEN and SOCS3. *Nature* **480**, 372–375 (2011).
6. R. Cartoni *et al.*, The mammalian-specific protein Armcx1 regulates mitochondrial transport during axon regeneration. *Neuron* **92**, 1294–1307 (2016).
7. Q. Han *et al.*, Restoring cellular energetics promotes axonal regeneration and functional recovery after spinal cord injury. *Cell Metab.* **31**, 623–641.e8 (2020).
8. C. Li, R. J. Samulski, Engineering adeno-associated virus vectors for gene therapy. *Nat. Rev. Genet.* **21**, 255–272 (2020).
9. D. M. Miller, S. D. Thomas, A. Islam, D. Muench, K. Sedoris, c-Myc and cancer metabolism. *Clin. Cancer Res.* **18**, 5546–5553 (2012).
10. S. M. Han, H. S. Baig, M. Hammarlund, Mitochondria localize to injured axons to support regeneration. *Neuron* **92**, 1308–1323 (2016).
11. T. Misgeld, M. Kerschensteiner, F. M. Bareyre, R. W. Burgess, J. W. Lichtman, Imaging axonal transport of mitochondria in vivo. *Nat. Methods* **4**, 559–561 (2007).
12. A. B. Knott, G. Perkins, R. Schwarzenbacher, E. Bossy-Wetzel, Mitochondrial fragmentation in neurodegeneration. *Nat. Rev. Neurosci.* **9**, 505–518 (2008).
13. S. Neumann, C. J. Woolf, Regeneration of dorsal column fibers into and beyond the lesion site following adult spinal cord injury. *Neuron* **23**, 83–91 (1999).
14. C. H. Ma *et al.*, Accelerating axonal growth promotes motor recovery after peripheral nerve injury in mice. *J. Clin. Invest.* **121**, 4332–4347 (2011).
15. F. M. Mar *et al.*, CNS axons globally increase axonal transport after peripheral conditioning. *J. Neurosci.* **34**, 5965–5970 (2014).
16. B. Zhou *et al.*, Facilitation of axon regeneration by enhancing mitochondrial transport and rescuing energy deficits. *J. Cell Biol.* **214**, 103–119 (2016).
17. S. Das, J. Boczan, C. Gerwin, P. B. Zald, Z. H. Sheng, Regional and developmental regulation of syntaphilin expression in the brain: A candidate molecular element of synaptic functional differentiation. *Brain Res. Mol. Brain Res.* **116**, 38–49 (2003).
18. C. H. Ma *et al.*, The BMP coreceptor RGMb promotes while the endogenous BMP antagonist noggin reduces neurite outgrowth and peripheral nerve regeneration by modulating BMP signaling. *J. Neurosci.* **31**, 18391–18400 (2011).
19. D. Wang *et al.*, A small molecule promotes mitochondrial fusion in mammalian cells. *Angew. Chem. Int. Ed. Engl.* **51**, 9302–9305 (2012).
20. V. B. Chine, N. P. B. Au, C. H. E. Ma, Therapeutic benefits of maintaining mitochondrial integrity and calcium homeostasis by forced expression of Hsp27 in chemotherapy-induced peripheral neuropathy. *Neurobiol. Dis.* **130**, 104492 (2019).
21. Y. M. Ho *et al.*, A lysosome-specific two-photon phosphorescent binuclear cyclometalated platinum(II) probe for in vivo imaging of live neurons. *Chem. Commun. (Camb.)* **50**, 4161–4163 (2014).
22. N. P. B. Au *et al.*, Ciguatoxin reduces regenerative capacity of axotomized peripheral neurons and delays functional recovery in pre-exposed mice after peripheral nerve injury. *Sci. Rep.* **6**, 26809 (2016).
23. V. B. Chine, N. P. B. Au, G. Kumar, C. H. E. Ma, Targeting Axon Integrity to Prevent Chemotherapy-Induced Peripheral Neuropathy. *Mol. Neurobiol.* **56**, 3244–3259 (2019).
24. A. Höke, Mechanisms of disease: What factors limit the success of peripheral nerve regeneration in humans? *Nat. Clin. Pract. Neurol.* **2**, 448–454 (2006).
25. Y. L. Weng *et al.*, An intrinsic epigenetic barrier for functional axon regeneration. *Neuron* **94**, 337–346.e6 (2017).
26. J. E. Shin, S. Geisler, A. DiAntonio, Dynamic regulation of SCG10 in regenerating axons after injury. *Exp. Neurol.* **252**, 1–11 (2014).
27. A. L. Kalinski *et al.*, Analysis of the immune response to sciatic nerve injury identifies efferocytosis as a key mechanism of nerve debridement. *eLife* **9**, e60223 (2020).
28. N. Bernard-Marissal *et al.*, Altered interplay between endoplasmic reticulum and mitochondria in Charcot-Marie-Tooth type 2A neuropathy. *Proc. Natl. Acad. Sci. U.S.A.* **116**, 2328–2337 (2019).
29. C. H. Ma, E. T. Bampton, M. J. Evans, J. S. Taylor, Synergistic effects of osteonectin and brain-derived neurotrophic factor on axotomized retinal ganglion cells neurite outgrowth via the mitogen-activated protein kinase-extracellular signal-regulated kinase 1/2 pathways. *Neuroscience* **165**, 463–474 (2010).
30. H. Chen *et al.*, Commensal microflora-induced T cell responses mediate progressive neurodegeneration in glaucoma. *Nat. Commun.* **9**, 3209 (2018).
31. C. H. E. Ma, J. S. H. Taylor, Trophic responsiveness of purified postnatal and adult rat retinal ganglion cells. *Cell Tissue Res.* **339**, 297–310 (2010).
32. K. K. Park *et al.*, Promoting axon regeneration in the adult CNS by modulation of the PTEN/mTOR pathway. *Science* **322**, 963–966 (2008).
33. V. Chandran *et al.*, A systems-level analysis of the peripheral nerve intrinsic axonal growth program. *Neuron* **89**, 956–970 (2016).
34. S. de Lima *et al.*, Full-length axon regeneration in the adult mouse optic nerve and partial recovery of simple visual behaviors. *Proc. Natl. Acad. Sci. U.S.A.* **109**, 9149–9154 (2012).
35. T. Kurimoto *et al.*, Long-distance axon regeneration in the mature optic nerve: Contributions of oncomodulin, cAMP, and pten gene deletion. *J. Neurosci.* **30**, 15654–15663 (2010).
36. T. Kurimoto *et al.*, Neutrophils express oncomodulin and promote optic nerve regeneration. *J. Neurosci.* **33**, 14816–14824 (2013).
37. A. R. Sas *et al.*, A new neutrophil subset promotes CNS neuron survival and axon regeneration. *Nat. Immunol.* **21**, 1496–1505 (2020).
38. X. W. Wang *et al.*, Lin28 signaling supports mammalian PNS and CNS axon regeneration. *Cell Rep.* **24**, 2540–2552.e6 (2018).
39. O. S. Dhande, B. K. Stafford, J. A. Lim, A. D. Huberman, Contributions of retinal ganglion cells to subcortical visual processing and behaviors. *Annu. Rev. Vis. Sci.* **1**, 291–328 (2015).
40. F. Bei *et al.*, Restoration of visual function by enhancing conduction in regenerated axons. *Cell* **164**, 219–232 (2016).
41. A. D. Güler *et al.*, Melanopsin cells are the principal conduits for rod-cone input to non-image-forming vision. *Nature* **453**, 102–105 (2008).
42. S. K. Chen, T. C. Badea, S. Hattar, Photoentrainment and pupillary light reflex are mediated by distinct populations of ipRGCs. *Nature* **476**, 92–95 (2011).
43. M. Yilmaz, M. Meister, Rapid innate defensive responses of mice to looming visual stimuli. *Curr. Biol.* **23**, 2011–2015 (2013).
44. X. Zhao, M. Liu, J. Cang, Visual cortex modulates the magnitude but not the selectivity of looming-evoked responses in the superior colliculus of awake mice. *Neuron* **84**, 202–213 (2014).
45. R. L. Morris, P. J. Hollenbeck, The regulation of bidirectional mitochondrial transport is coordinated with axonal outgrowth. *J. Cell Sci.* **104**, 917–927 (1993).
46. Y. Zhang *et al.*, Elevating growth factor responsiveness and axon regeneration by modulating presynaptic inputs. *Neuron* **103**, 39–51.e5 (2019).
47. T. L. Lewis Jr., G. F. Turi, S. K. Kwon, A. Losonczy, F. Polleux, Progressive decrease of mitochondrial motility during maturation of cortical axons in vitro and in vivo. *Curr. Biol.* **26**, 2602–2608 (2016).
48. D. C. Chan, Mitochondrial dynamics and its involvement in disease. *Annu. Rev. Pathol.* **15**, 235–259 (2020).
49. A. Misko, S. Jiang, I. Wegorzewska, J. Milbrandt, R. H. Baloh, Mitofusin 2 is necessary for transport of axonal mitochondria and interacts with the Miro/Milton complex. *J. Neurosci.* **30**, 4232–4240 (2010).
50. R. H. Baloh, R. E. Schmidt, A. Pestronk, J. Milbrandt, Altered axonal mitochondrial transport in the pathogenesis of Charcot-Marie-Tooth disease from mitofusin 2 mutations. *J. Neurosci.* **27**, 422–430 (2007).
51. M. Ding *et al.*, Mitochondrial fusion promoter restores mitochondrial dynamics balance and ameliorates diabetic cardiomyopathy in an optic atrophy 1-dependent way. *Acta Physiol. (Oxf.)* **229**, e13428 (2020).
52. L. Dong *et al.*, Promotion of mitochondrial fusion protects against developmental PBDE-47 neurotoxicity by restoring mitochondrial homeostasis and suppressing excessive apoptosis. *Theranostics* **10**, 1245–1261 (2020).
53. V. Cavallucci *et al.*, Acute focal brain damage alters mitochondrial dynamics and autophagy in axotomized neurons. *Cell Death Dis.* **5**, e1545 (2014).
54. K. C. O'Donnell, M. E. Vargas, A. Sagasti, S. Wld, WldS and PGC-1α regulate mitochondrial transport and oxidation state after axonal injury. *J. Neurosci.* **33**, 14778–14790 (2013).
55. F. M. Nathan *et al.*, Upregulating Lin28a promotes axon regeneration in adult mice with optic nerve and spinal cord injury. *Mol. Ther.* **28**, 1902–1917 (2020).
56. S. Li *et al.*, Injured adult retinal axons with Pten and Socs3 co-deletion reform active synapses with suprachiasmatic neurons. *Neurobiol. Dis.* **73**, 366–376 (2015).
57. X. Luo *et al.*, Three-dimensional evaluation of retinal ganglion cell axon regeneration and pathfinding in whole mouse tissue after injury. *Exp. Neurol.* **247**, 653–662 (2013).
58. R. Cartoni, G. Pekkurnaz, C. Wang, T. L. Schwarz, Z. He, A high mitochondrial transport rate characterizes CNS neurons with high axonal regeneration capacity. *PLoS One* **12**, e0184672 (2017).
59. J. H. Lim *et al.*, Neural activity promotes long-distance, target-specific regeneration of adult retinal axons. *Nat. Neurosci.* **19**, 1073–1084 (2016).
60. D. L. Rousso *et al.*, Two pairs of ON and OFF retinal ganglion cells are defined by intersectional patterns of transcription factor expression. *Cell Rep.* **15**, 1930–1944 (2016).
61. F. Wang, E. Li, L. De, Q. Wu, Y. Zhang, OFF-transient alpha RGCs mediate looming triggered innate defensive response. *Curr. Biol.* **31**, 2263–2273.e3 (2021).
62. L. Satarian *et al.*, Intravitreal injection of bone marrow mesenchymal stem cells in patients with advanced retinitis pigmentosa: A safety study. *J. Ophthalmic Vis. Res.* **12**, 58–64 (2017).
63. D. V. Do, W. Rhoades, Q. D. Nguyen, Pharmacokinetic study of intravitreal aflibercept in humans with neovascular age-related macular degeneration. *Retina* **40**, 643–647 (2020).